Prediction of distinct surface segregation effects due to coordination-dependent bond-energy variations in alloy nanoclusters

Leonid Rubinovich and Micha Polak*
Department of Chemistry, Ben-Gurion University, Beer-Sheva 84105, Israel
(Received 30 March 2009; revised manuscript received 27 May 2009; published 7 July 2009)

The first implementation of a recently introduced method based on the extraction of the coordination dependence of surface bond-energy variations (CBEV) from density-functional theory (DFT) computed pure-metal surface-energy anisotropy is reported. In particular, polynomial functions fitted to DFT data computed previously for Pt, Pd, and Rh are used as input energetics for statistical-mechanical computations of Pt-Pd 923-atom cuboctahedron-cluster compositional structures (and Pt-Rh(111) as a test case) using the free-energy concentration expansion method (FCEM). The major findings concern the roles of preferential strengthening of intrasurface and surface-subsurface interlayer bonds leading to quite unique segregation characteristics: (i) strong Pt segregation at certain (111) surface sites of the Pt-Pd clusters, accompanied, at relatively high overall Pt composition, by weaker Pt segregation forming Pt-Pd ordered (100) structure, whereas Pd segregates mainly at the edge and vertex sites; (ii) dominant Pd subsurface segregation. The high computation efficiency of the CBEV/FCEM approach allows the determination of the complete temperature dependence of atomic-exchange processes among surface sites, as well as between subsurface and deeper sites, reflected in the corresponding configurational heat-capacity curves. Compared to other approaches, the high transparency of this method helps to elucidate the origin of the distinct bond-energy-variation effects on site-specific segregation in alloy nanoclusters.

DOI: 10.1103/PhysRevB.80.045404 PACS number(s): 61.46.Df, 68.35.Dv, 82.60.Qr, 68.35.Md

I. INTRODUCTION

Considerable efforts have been made to model compositional and geometrical structures specific to alloy nanoclusters compared to the corresponding bulk alloys, with emphasis on the outer surface shell.[1] These theoretical-computational studies are motivated by the relevance of chemical and physical properties, which depend on the cluster structure and size, for applications in catalysis, magnetic media, or electronic devices. Pt-Pd and Pt-Rh modeled in this work are widely used as catalysts in the detoxication of car exhaust gases. Limitations of current experimental characterization techniques make modeling almost the only tool to obtain atomic-scale geometrical and compositional information concerning nanosized alloy clusters. Several approaches that differ in the level of accuracy and efficiency have been reported in the literature.[1] In particular, as far as energetics are concerned, the currently most common methods are based either on the density-functional theory (DFT) or on empirical (or semiempirical) many-body potentials (EP) such as the second moment approximation to the tight-binding theory (TB-SMA), or preferably, on a combination of both.[2] The former can be of high accuracy but the rather time consuming computations limit their practical applicability to relatively small size alloy clusters. For the study of medium or large clusters the generally less accurate (but computationally much more efficient) EP methods have been often used. For the exploration of cluster properties at finite temperatures, the interatomic energetics has to be combined with thermodynamic/statistical-mechanical formalism or computer simulations. Employing statistical-mechanical explicit expressions for the alloy free energy has certain advantages. In particular, the free-energy concentration expansion method (FCEM), which takes into account short-range order (SRO) (Ref. 3) in a system of equilibrated atom-exchanging clusters, has proven to be highly efficient in computation of site-specific concentrations (obtainable by F minimization) vs overall composition, temperature and cluster size,[4] as compared to Monte Carlo simulations, for example.

Our first attempts to go beyond simple empirical energetics as input in the FCEM for the study of alloy nanoclusters incorporated[4,5] elemental bond energies and their surface-induced variations as obtained by means of the Naval Research Laboratory-tight-binding method (NRL-TB).[6] However, it appears that quantitative evaluation of the role of elemental bond-energy variations in surface segregation in bulk alloys and alloy clusters necessitates more reliable energetics. Therefore, we introduced most recently another approach to the issue of near-surface interatomic bonding.[7] Our aim was to develop a DFT-based method of high efficiency, namely, to retain a reasonable accuracy in relatively fast computations of medium- and large-cluster compositional structures. The idea was to derive a procedure for extracting the coordination dependence of intrasurface and surface-subsurface pair-bond-energy variations (CBEV) from DFT-computed surface-energy anisotropy.

The paper is organized as follows. After describing briefly the introduced method, the results computed for Pt-Pd 923-atom clusters are divided between surface and subsurface segregation effects. Pd clusters of this size were predicted to have the cuboctahedron (Oh) shape.[8] Computational vs experimental data for segregation in $Pt_{0.25}Pd_{0.75}(111)$ are given as a test case. The discussion deals with the origins of the two respective driving forces in the context of bond-energy variations involving the two outer shells and assesses previous theoretical and experimental studies of the Pt-Pd system. A summary of the research results and prospects concludes the article.

II. METHODOLOGY

The surface energy can be written in terms of nearest-neighbor (NN) pair-bond-energy variations, δw_{mn}, relative to the reference bulk value, w_b, and the number of broken bonds ΔZ_m around site m, as[5,7]

$$E_s = \sum_m \gamma_m = \sum_m \frac{1}{2}\left(\sum_{n(n\neq m)} \delta w_{mn} - \Delta Z_m w_b \right), \quad (1)$$

where γ_m denotes the "m-site tension." Polynomial functions are fitted to DFT-computed E_s data of the pure metals, thus furnishing the bond-energy variations. In particular, for an $m-n$ bond with ΔZ_m and ΔZ_n NN broken bonds at the m and n sites, the variation δw_{mn}, is considered as a function of two bond-coordination variables, namely, a "symmetric" one, $x_{mn}=\Delta Z_m+\Delta Z_n$, taking into account the total number of broken bonds and an "antisymmetric" variable, $y_{mn}=\Delta Z_m - \Delta Z_n$. The latter takes into account possible nonequivalency of the two sites corresponding mostly to surface-subsurface interlayer contributions. In our previous study,[7] six DFT-computed surface energies[9] for each of the Pt, Pd, and Rh metals were mapped into arrays of six coefficients of polynomials of sequentially ascending powers of the coordination variables,

$$\delta w_{mn} = a_{1,0}x_{mn} + a_{2,0}x_{mn}^2 + a_{0,2}y_{mn}^2 + a_{3,0}x_{mn}^3 + a_{1,2}x_{mn}y_{mn}^2 + a_{4,0}x_{mn}^4. \quad (2)$$

In this way, the energy variations are treated as coordination-dependent functions rather than numerical values. This approach helps to circumvent transferability problems, namely, the need to repeat fitting of interactions for every specific surface geometry. It can be noted that in the present approach, any preliminary assumptions concerning bond variations are absent and the polynomial function is chosen due to its generality and simplicity. Furthermore, odd powers of y_{mn} are omitted because of symmetry considerations ($\delta w_{mn} = \delta w_{nm}$).

The derived bond-energy variation is added to the bulk value to give the intrasurface or the surface-subsurface pair-bond energies, $w_{mn}=w_b+\delta w_{mn}$, which are fully compatible with the FCEM. The new approach is particularly valid when the mixing energy, related to the effective heteroatomic interaction between constituents I and J, $V=\frac{1}{2}(w^{II}+w^{JJ}-2w^{IJ})$, is relatively small or nearly independent of coordination. Since this parameter and the atomic-size mismatch are small for both alloys (8 and 9 meV and ~3% and ~1% for Pt-Rh and Pt-Pd, respectively), segregation effects of elemental bond-energy variations alone are anticipated.

It should be noted that experimental cohesive energies have been quite often used as bulk energies, E_b ($=6w_b$ in fcc metals) in semiempirical or empirical modeling of properties of transition metals and their alloys [e.g., in TB-SMA (Ref. 10 and 11)], thus neglecting the free-atom spin-polarization and promotion energy contributions.[12,13] The importance of employing corrected cohesive energies for avoiding erroneous results was demonstrated recently for Pt and Rh in Pt-Rh clusters.[14] The corrections for Pd and Pt are shown in Fig. 1 together with Pd bulk-energy values calculated directly using

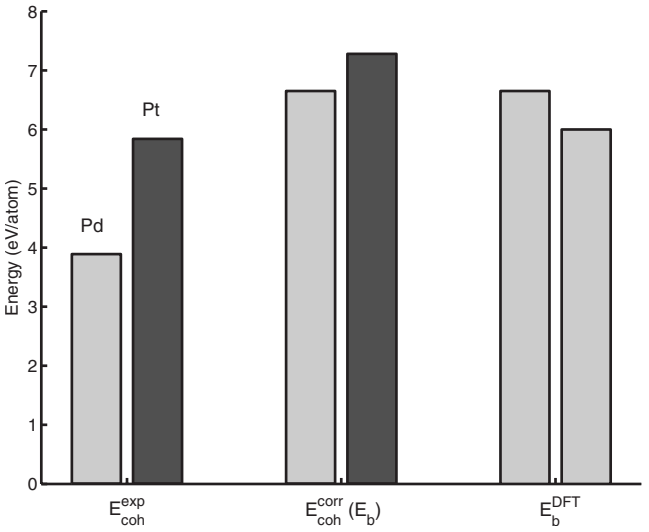

FIG. 1. Palladium and platinum experimental (Ref. 35) and corrected cohesive energies (Ref. 13) together with DFT-computed Pd bulk energies according to Moriarty (Ref. 15) (left) and Methfessel *et al.* (Ref. 16) (right).

DFT methods.[15,16] The latter agree quite well with the corrected value, all deviating significantly from the experimental cohesive energies.

The derived surface-subsurface interlayer as well as intrasurface bond-energy variations exhibit the expected general tendency to increase for lower coordinations (Fig. 2). In spite of the overall similar shape of the δw_{mn} curves obtained for the two metals, there are certain differences which, as described below, can lead to remarkable compositional-

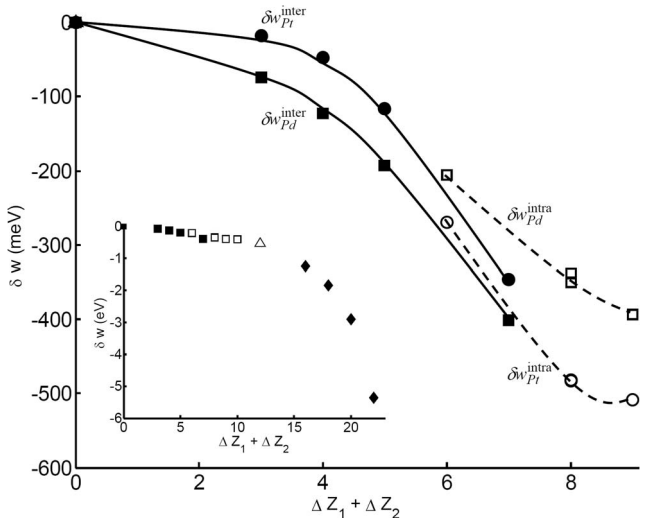

FIG. 2. The coordination dependence of surface-subsurface (filled marks) and intrasurface (open marks) bond-energy variations for elemental Pd (squares) and Pt (circles) as extracted from DFT-reported surface energies. Note the reversal in relative strengthening of the Pd and Pt interbonds vs intrabonds, namely, $|\delta w_{\mathrm{Pd}}^{\mathrm{inter}}| > |\delta w_{\mathrm{Pt}}^{\mathrm{inter}}|$ is consistent with $|\delta w_{\mathrm{Pd}}^{\mathrm{intra}}| < |\delta w_{\mathrm{Pt}}^{\mathrm{intra}}|$. Inset: the Pd Oh vertex-edge bond-energy variation (12 pair-missing bonds, triangle) is obtained by additional fitting (Ref. 7) to lower-coordinated bonds of small clusters (16–22 pair-missing bonds, diamonds).

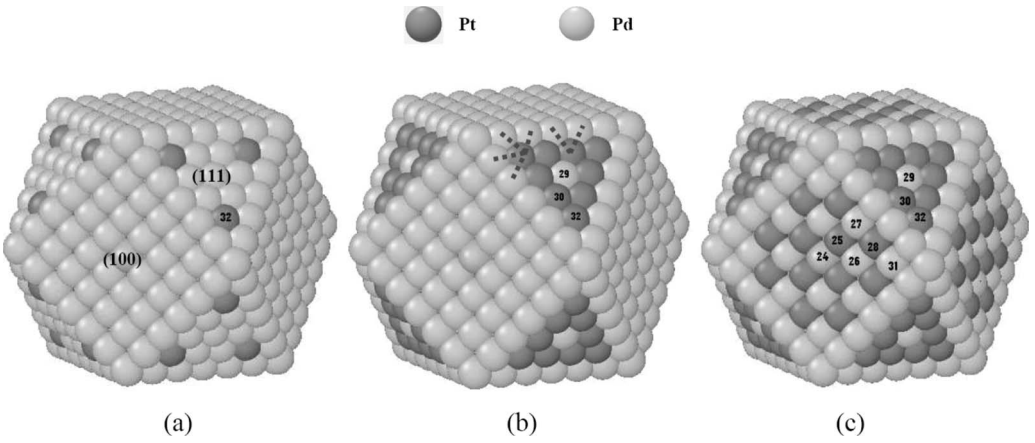

FIG. 3. CBEV/FCEM-computed surface compositional structures of Pt-Pd 923-atom Oh clusters at low T: (a) $c_{Pt}=24/923$, (b) $c_{Pt}=195/923$, and (c) $c_{Pt}=357/923$ ("magic numbers"). (111)-edge bonds are marked.

structure phenomena. While the above variations were derived for plane surfaces with overall numbers of missing bonds per pair, x, up to 10, for the case of nanoclusters energy variations in lower-coordinated bonds are often needed. For this, the coefficients of the polynomial were also fitted[7] to DFT-computed energies of small Pd and Pt clusters[17,18] (dimer, triangle, tetrahedron, and octahedron, see inset of Fig. 2).

III. RESULTS

The elemental bond-energy variations are implemented in CBEV/FCEM computations of 923-atom Pt-Pd Oh clusters having different overall compositions for a wide range of temperatures. These variations have significant effects on the surface as well as the subsurface segregation driving forces, namely, to a large extent they determine the surface compositional structure and the near-surface site-specific composition profiles.

A. Surface compositional structures

CBEV effects on the low-temperature segregation are introduced first for Pt-dilute clusters, such as Pt_1Pd_{922} up to $Pt_{24}Pd_{899}$. Quite surprisingly, at certain surface sites, segregation of platinum is predicted, whereas generally Pd is the segregating element in Pt-Pd bulk alloys, in accordance with the Pd lower surface energies.[9] In particular, sites no. 32 at the corners of the Oh (111) faces are exclusively populated by Pt [Fig. 3(a)]. This segregation reversal is attributed to a significant strengthening of particular Pt-Pt surface bonds compared to Pd-Pd bonding that makes occupation of these surface sites by Pt energetically advantageous, as is further discussed quantitatively below. With increased overall Pt content beyond 24 atoms, distinct sites are gradually populated. In clusters with 25–117 Pt atoms, an $L1_2$-type order arises in the 309-atom cuboctahedral inner core, followed by population of sites no. 30 (and more core sites) between 118 and 195 Pt atoms [Fig. 3(b)]. Then other inner sites are occupied by Pt and from $Pt_{271}Pd_{662}$ the cluster surface starts again to be populated by Pt [at (100) alternate sites], until for $Pt_{357}Pd_{566}$ another centrosymmetrically ordered compositional structure forms [Fig. 3(c)]. It consists of five shells, $(Pd+Pt)_{surf}$-Pd-Pt-(Pd+Pt)-Pt-Pd, surrounding a central Pt atom (compared, for example, to a 3-shell Pd_{surf}-Pt-Pd structure predicted by the TB-SMA for the $Pd_{56}Pt_{42}$ Leary tetrahedron[19]).

Raising the temperature results in a rich pattern of site exchange surface processes. Their full temperature dependence [for the latter cluster, Fig. 4(a)] reveals the corresponding sites and reflects the relative stability of the low-temperature-segregated sites. Thus, a rather sharp Pt-Pd disordering transition involves the (100) sites at about 100 K, whereas exchange between the more stable Pt-segregated sites no. 30 and the Pd-segregated sites no. 29 at (111) spreads over a much wider temperature range. Exchange between the even more stable Pt-segregated site no. 32 and edge sites decorated by Pd alone starts at higher temperatures. The thermally most stable sites are clearly the Pd-occupied low-coordinated vertices, exhibiting a delayed exchange with (111) sites. The segregation energetics pertinent to the (100) and particularly to the (111) sites are discussed below in terms of site-specific preferential bond strengthening. Given the computed site concentrations as function of temperature, the configurational heat capacity associated with the diverse heat-consuming processes can be readily computed, as we reported for other alloy nanoclusters.[20] Three distinct Schottky-type peaks can be noted in Fig. 4(b): a relatively broad one with maximum at about 500 K corresponds to the (111) site exchange processes spreading over quite a wide range of temperatures, a central sharp peak at about 100 K that corresponds to the less energetic (100) site exchange, and a least energetic very sharp peak at about 30 K due to Pt-Pd transition involving inner-core sites. The appearance of the second peak at higher temperature seems to reflect a combination of the strengthened bonds at the (100) face, compared to the core bond energy, with contributions from the exothermic Pd-Pt ordering tendency, involving also the Pd-rich subsurface (discussed below). It can be noted that experimental measurements of such cluster caloric curves (if possible) could confirm the theoretical predictions concerning the nature of exchange processes occurring in the cluster. Possible disagreements might indicate kinetic limitations (es-

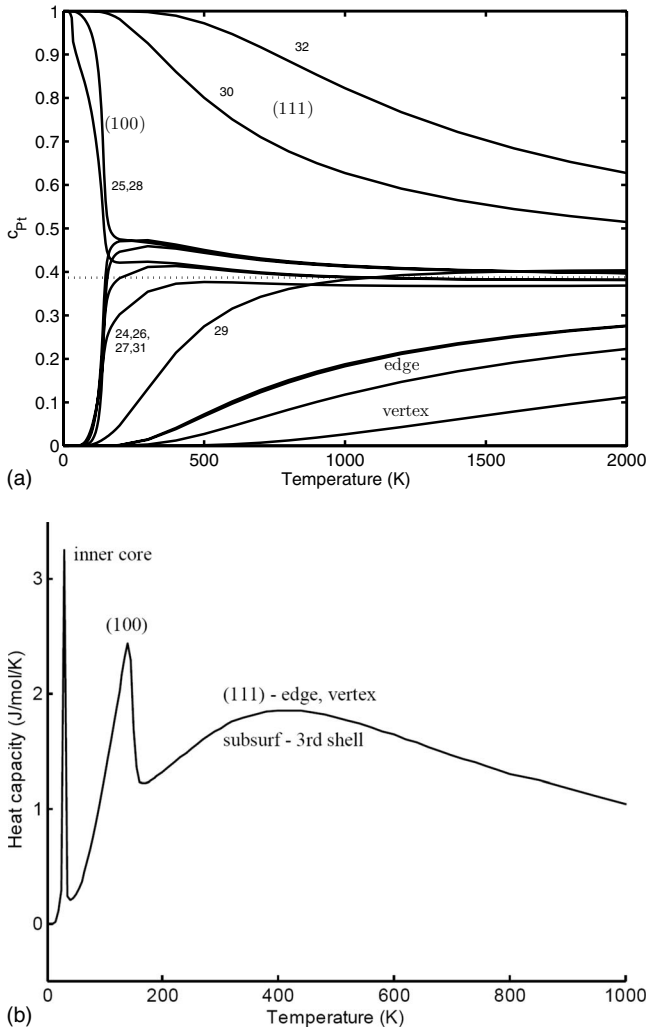

FIG. 4. (a) Surface-site compositions as function of temperature for the $Pt_{357}Pd_{566}$ Oh cluster (site numbering as in Fig. 3). Dotted line is overall cluster composition. (b) The corresponding configurational heat-capacity curve due to atomic-exchange processes computed with all 923 site concentrations as input.

pecially at low temperatures) or the need to improve the modeling. In the absence of computations, only tentative assignments of the peaks can be made on the basis of the underlying relative energetics (peak temperatures) and their height and width.

B. Surface-subsurface composition profiles

While intralayer bond-energy variations play a major role in the site-specific compositional structure of the Pt-Pd cluster surface, the near-surface composition profile is expected to be affected mainly by bond-energy variations between surface and subsurface atoms. Experimental measurement of atomic-scale layer-by-layer compositions is tedious even for flat surfaces and is limited to very few dedicated techniques, thus making such computations quite essential, especially for clusters. This section starts with presenting computation results of average shell compositions for $Pt_{357}Pd_{566}$, followed by computations for a (100)-face site-specific profile that is

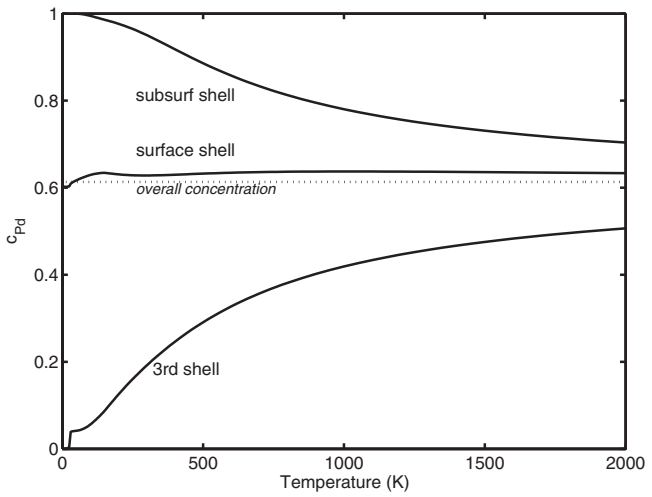

FIG. 5. Average compositions of the three outer shells vs T computed for the $Pt_{357}Pd_{566}$ Oh cluster.

compared to $Pt_{0.25}Rh_{0.75}$ (111). As a test case, the latter profile is compared to a reliable experimental profile reported in the literature.[21]

Figure 5 shows the three outer-shell average compositions as a function of temperature. Relative to a very weak Pd-surface segregation, its segregation at the subsurface is dominant and prevails also in clusters having other overall compositions. The Pd-rich subsurface shell exchanges Pt atoms coming from the Pt-rich third shell underneath with increasing temperature, whereas the slightly Pd-segregated surface (average composition) remains nearly unchanged. The latter feature is consistent with exchange processes occurring among surface sites [see Fig. 4(a)] and no desegregation to the cluster core. The subsurface third-shell exchange processes contribute to the high-temperature broad Schottky peak [Fig. 4(b)]. Example of a site-specific profile is given for site no. 24 at the center of the cluster (100) face (Fig. 6). The results for 140 K clearly exhibit quite a unique segregation profile with pure-Pd subsurface, followed by a strongly

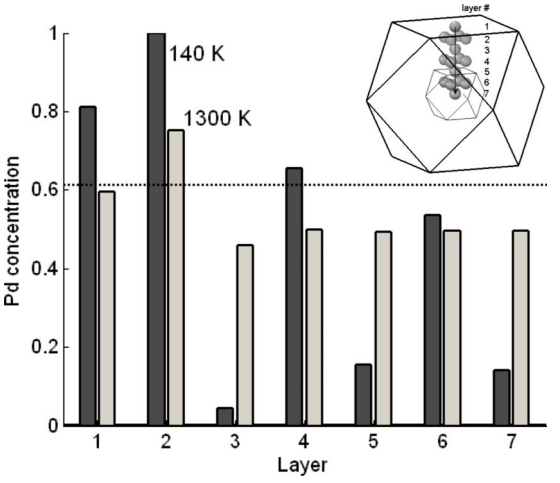

FIG. 6. Layer-by-layer composition profiles computed for low and high temperatures starting from the center of the $Pt_{357}Pd_{566}$ Oh (100) face (site no. 24). Dotted line is overall cluster composition.

Pd-depleted third layer and relatively more moderate compositional oscillations in the next four shells, which are associated with the ordering tendency of this alloy. The Pd concentrations of the three last shells are below its overall composition due to the limited content of Pd atoms in the cluster (compared to the practically infinite reservoir in case of bulk alloy surface segregation). The 1300 K profile shows significant entropic mixing among the shells and it is instructive to compare it with the $Pt_{0.25}Rh_{0.75}$ (111) profile given in Fig. 7. In particular, unlike the Pt-Pd case, in Pt-Rh the subsurface is strongly depleted in the surface segregating element (Pt) resulting in a surface-subsurface oscillatory profile. As discussed in detail below, this distinct behavior demonstrates once again the important role of near-surface bond-energy variations. The CBEV/FCEM computations for $Pt_{0.25}Rh_{0.75}$ (111) are in very good agreement with reported experimental data of the highly sensitive middle energy ion scattering (MEIS) method[21] (Fig. 7). Their accuracy is further proven by the close similarity to predictions based on the cluster expansion technique in conjunction with DFT.[22,23]

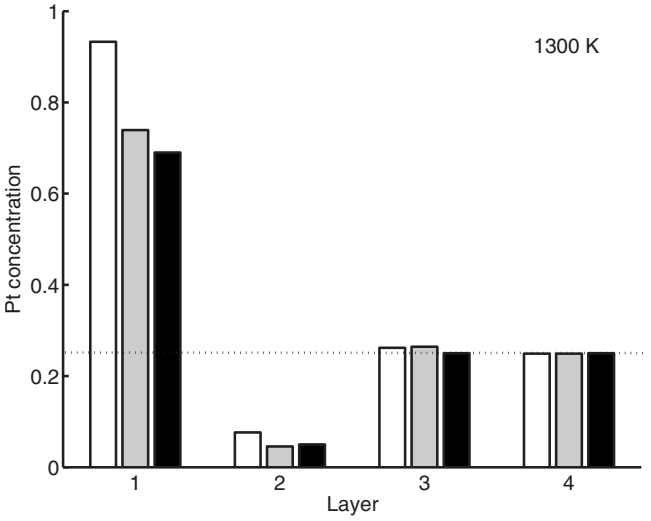

FIG. 7. Composition profiles computed for $Pt_{25}Rh_{75}$(111) with the CBEV energetics (gray bars) and with the NRL-TB energetics (Ref. 5) (white bars) together with MEIS experimental data (Ref. 21) (black bars) (1300 K). Dotted line is overall bulk composition.

IV. DISCUSSION

The computed results distinctly highlight the role of preferential strengthening of surface bonds in inducing remarkable segregation phenomena at the surfaces and subsurfaces of alloy nanoclusters in particular. Generally, when intrasurface or surface-subsurface bonds of one element get significantly stronger than the other element bonding, the former element can enrich the corresponding surface or subsurface. Thus, the CBEV/FCEM results shown above for the Pt-Pd cluster can be understood in a straightforward way by analyzing such differences [based on Eq. (1)] as estimation of the segregation driving force to an outer-surface site m,

$$\Delta^{\text{Pd-Pt}}(\gamma_{m\in 1}) \equiv \gamma^{\text{Pd}}_{m\in 1} - \gamma^{\text{Pt}}_{m\in 1} = \frac{1}{2}\left(\sum_{n(n\neq m)} \Delta^{\text{Pd-Pt}}(\delta w_{mn}) - \Delta Z_m \Delta^{\text{Pd-Pt}}(w_b)\right), \tag{3}$$

and to a fully coordinated subsurface site,

$$\Delta^{\text{Pd-Pt}}(\gamma_{m\in 2}) \equiv \gamma^{\text{Pd}}_{m\in 2} - \gamma^{\text{Pt}}_{m\in 2} = \frac{1}{2}\sum_{n(n\neq m)} \Delta^{\text{Pd-Pt}}(\delta w_{mn}), \tag{4}$$

where

$$\Delta^{\text{Pd-Pt}}(\delta w_{mn}) \equiv \delta w^{\text{Pd}}_{mn} - \delta w^{\text{Pt}}_{mn} \text{ and } \Delta^{\text{Pd-Pt}}(w_b) \equiv w^{\text{Pd}}_b - w^{\text{Pt}}_b. \tag{5}$$

As shown in the following, for both cases the origins of the CBEV/FCEM-computed segregation effects can be elucidated via the $\Delta^{\text{Pd-Pt}}(\gamma_m)$ signs. In particular, the balance of the two contributions to the surface segregation driving force [Eq. (3)], namely, the bond-variation-related first term and the usual bond-breaking second term, determines the segregation tendency, namely, Pd or Pt segregation. Thus, high-coordination sites adjacent to several low-coordinated sites might exhibit segregation reversal, provided the preferential strengthening is strong enough. For subsurface segregation, only the bond-variation first term prevails [Eq. (4)].

A. Role of intrasurface bonding variations

The strengthening of intrasurface surface bond energies is systematically larger for Pt compared to Pd [Fig. 8(a)] and hence γ^{Pt}_m is lowered more significantly, especially for sites no. 30 and no. 32 with edge-(111) bonds [see Fig. 3(b)]. Applying Eq. (3) to these sites shows that the value of the term involving $\Delta^{\text{Pd-Pt}}(\delta w_{mn})$ is larger than that of $\Delta^{\text{Pd-Pt}}(w_b)$, resulting in positive $\Delta^{\text{Pd-Pt}}(\gamma_{m=30,32})$ values (Table I), namely, a reversal to Pt segregation, as obtained by the full CBEV/FCEM calculations (see Figs. 3 and 4). Since site no. 32 has twice more edge-(111) bonds [Fig. 3(b)], the Pt-segregation driving force is significantly larger (Table I), in agreement with the relatively delayed Pt depopulation of this site with increasing temperature [see Fig. 4(a)]. It should be noted that unlike the common tendency, the most energetically favorable face for Pt segregation is the closed packed (111) face, and not the more open (100) (see Figs. 3 and 4). This "anomaly" is related to the unique driving force in the present case, namely, the preferential strengthening of surface bonds. Although the strengthening magnitude is predicted to be the same, e.g., for (100)-(100) and (111)-edge [Fig. 8(a)], the overall larger number of bonds in the more dense (111) face still renders it energetically favorable. Regarding site no. 29, the smaller relative variation in (111)-(111) bonding, $\Delta^{\text{Pd-Pt}}(\delta w_{mn})$ [Fig. 8(a)], keeps $\Delta^{\text{Pd-Pt}}(\gamma_{m=29})$ negative (Table I), i.e., Pd is expected to segregate to this site. Since V in this system is very small, the heteroatomic Pt-Pd bond energies are close to the average of the corresponding Pt-Pt and Pd-Pd bond energies, as are their variations at the surface $|\delta w^{\text{Pd-Pt}}| \approx \frac{1}{2}(|\delta w^{\text{Pd-Pd}}| + |\delta w^{\text{Pt-Pt}}|) > |\delta w^{\text{Pd-Pd}}|$. Hence, the Pt-Pd bonds preferentially strengthen along with the Pt-Pt bonds, and the above arguments should

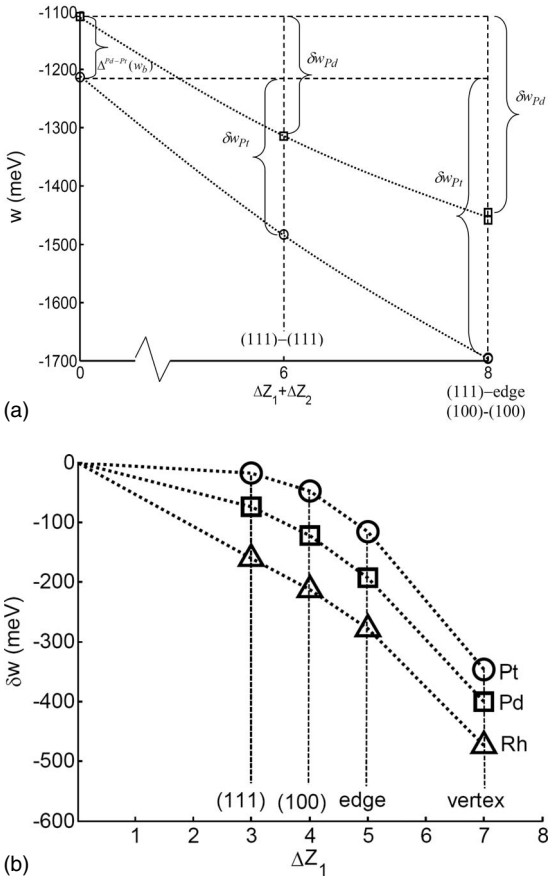

FIG. 8. (a) CBEV surface bond energies of Pd (squares) and Pt (circles) vs the number of pair missing bonds for the indicated sites. The pertinent variations δw^{intra} (given in Fig. 2) are marked. The magnitude of the δw difference relative to that of w_b determines to a large extent the segregating element (Pd or Pt). (b) Surface-subsurface bond-energy variations δw^{inter} of elemental Pt, Pd, and Rh for the Oh indicated surface sites having ΔZ_1 missing bonds.

hold also for this bonding that is stabilized at the surface (e.g., Fig. 3).

This cluster system has been studied previously using different modeling approaches but usually no segregation reversal to Pt was reported. At least, part of the exclusive Pd-segregation predictions seem to be associated with the use of uncorrected cohesive energies for fitting of parameters in empirical or semiempirical potentials. For example, this was done in a simplistic bond order simulation (BOS) modeling[24] and in a recent advanced study of 38-atom Pd-Pt clusters that used the Gupta potential based on the TB-SMA combined with DFT (Ref. 25) (although in the latter case the small cluster size may partially account for the difference in the predicted segregation tendency). Similarly, TB-SMA was used to study a variety of other Pd-Pt clusters exhibiting Pd segregation.[19,26] Regarding the discrepancy in the predicted segregation tendency, we performed further computations that ignore the estimated corrections of 2.76 and 1.44 eV to the respective Pd and Pt experimental cohesive energies (see Fig. 1). This leads to a larger $\Delta^{\text{Pd-Pt}}(w_b)$ contribution resulting [via Eq. (3)] in Pd segregation at *all* surface sites. In a recent EP/molecular dynamics (MD) study, the segregation tendency to the surfaces of supported nanoparticles was predicted to be dependent on their overall composition and size.[27] It should be recalled that in spite of the present prediction (using correct bulk energies) of distinct Pt segregation at certain surface sites, the average surface composition of Pd (for non-Pt-dilute clusters) is still slightly above the cluster overall composition and together with the subsurface shell strong Pd enrichment, it signifies overall Pd segregation, which seems to be in agreement with the lower surface energies of this metal.[9]

TABLE I. Estimation of segregation driving forces to the (111) surface sites in Pt-Pd 923 Oh cluster.

	Site no. (m)		
Site tension (eV)	29	30	32
γ_m^{Pd}	0.9338	0.7894	0.6450
γ_m^{Pt}	0.9840	0.7723	0.5606
$\Delta^{\text{Pd-Pt}}(\gamma_m)$	−0.0503	0.0171	0.0843

TABLE II. Estimation of segregation driving forces to the (100) surface site no. 24 (and to the subsurface sites below it) in Pt-Pd 923 Oh cluster (top) and to the (111) surface and subsurface in Pt-Rh (bottom).

		Layer no.	
Surface	Site tension (eV)	1	2
Pt-Pd	γ_m^{Pd}	1.2946	−0.2456
(100)	γ_m^{Pt}	1.3664	−0.0944
$m=24$	$\Delta^{\text{Pd-Pt}}(\gamma_m)$	−0.0718	−0.1510
	γ_m^{Pt}	0.9839	−0.0269
	γ_m^{Rh}	1.2741	−0.2401
Pt-Rh(111)	$\Delta^{\text{Pt-Rh}}(\gamma_m)$	−0.2902	0.2132

B. Role of surface-subsurface bonding variations

The composition of the subsurface in this alloy system is determined primarily by preferential variations in the surface-subsurface bonding (and to a lesser extent by the small mixing tendency expressed by V). Opposite to the intrasurface case [Fig. 8(a)], the interlayer bond-energy variations are systematically larger in Pd compared to Pt [Fig. 8(b)], leading to Pd enrichment in all the subsurface sites (see Fig. 5). The basic energetics for the cluster (100) central site [no. 24, Fig. 3(c)], derived by using the CBEV data in Eqs. (3) and (4), are summarized in Table II (upper part). Clearly, the driving force for Pd segregation [$\Delta^{\text{Pd-Pt}}(\gamma_m)$] is much larger for the subsurface site in accordance with the FCEM-computed profiles (Fig. 6). The entirely different profile obtained for Pt-Rh (111) (Fig. 7) is due to Rh having considerably stronger interlayer bond-energy variations compared to Pt [Fig. 8(b)]. Consequently, Rh segregates to the subsurface, while Pt, due to its lower bulk bond energy (and preferential strengthening of its intrasurface bonds) segregates to the surface layer, resulting in a strongly oscillatory

profile. Similar arguments have been introduced in our previous work based on the NRL-TB/FCEM approach[5] emphasizing that in alloys with a weak mixing tendency, such as Pt-Rh, it cannot be the origin of high-temperature oscillations. Hence, it arises from the opposite signs of the segregation driving forces $\Delta^{\text{Pt-Rh}}(\gamma_m)$ for the surface vs subsurface layers (Table II, bottom). On the other hand, in case of site no. 24 in Pd-Pt(100), $\Delta^{\text{Pd-Pt}}$ has the same (negative) sign for the two layers (Table II, upper part).

Different near-surface profiles were reported before for Pt-Pd flat surfaces. Rousset *et al.*[28] formulated a theory of segregation using the equivalent-medium approximation and bond-strength modifications at surfaces. Unlike the present CBEV results, an oscillatory Pd-surface Pt-subsurface profile is predicted due to dominant Pd strengthening rather than that of Pt. However, the accuracy of such an approach seems to be questionable since it is based on the semiempirical TB-SMA method with uncorrected cohesive energies and the use of an empirical second-order polynomial for the coordination dependence of site energies. Likewise, questionable is the accuracy of effective-medium-theory (EMT) calculations of Pt-Pd spherically truncated clusters[29] and of TB-SMA based calculations of icosahedral and decahedral 55-atom Pt-Pd clusters.[30] Both studies are based on empirical parameters such as the experimental cohesive energies[31] and predict Pt subsurface segregation. On the other hand, the same work[29] reports DFT-local-density-approximation calculations of the (111) surface with Pd surface segregation and slight Pd subsurface segregation at high temperatures, in general agreement with DFT-generalized-gradient-approximation calculations of the Pd segregation energy in this system.[32]

As far as experimental data are concerned the situation is even more ambiguous. First, obviously no current technique can furnish atomic-scale compositional structures of nanocluster surface and subsurface (e.g., Figs. 3–5). Reported extended x-ray-absorption fine-structure (EXAFS) measurements yielded some average coordination numbers for zeolite-supported Pt-Pd catalysts[29] with Pd enrichment at the surface. However, segregation in inner sites was not ruled out and the EXAFS experiments were carried out in a hydrogen atmosphere. In a photoemission study of $Pt_{50}Pd_{50}(111)$,[33] the reported oscillatory Pd-surface Pt-subsurface profile seems to be questionable due to the apparently insufficient annealing time and inaccuracies involved in the spectral deconvolution procedure. Likewise, results of low-energy ion scattering spectroscopy (LEIS) measurements of Pt-Pd nanoclusters obtained by laser vaporization[34] are inconclusive due to the use of poor UHV, extensive ion sputtering and unclear equilibration conditions.

In short, the experimental studies and many of the theoretical studies of Pd-Pt clusters suffer from several drawbacks that render their validity and accuracy quite uncertain. On the other hand, the main predictions of the present DFT-based study are supported by the successful Pt-Rh test case using the same approach. Moreover, the accuracy of the CBEV method is confirmed by reasonably low cross-validation scores (~2%) obtained for surface energies of each of the three elements.[7]

V. CONCLUSIONS

This research involves two distinct goals. The first, reported in our previous publication and briefly addressed here, is the formulation of a physically transparent approach to metal surface energetics, incorporating CBEV extracted from DFT-based data. By the use of polynomial coordination functions, the CBEV method can provide transferability of energetic parameters in different surface geometries and cluster structures and is expected to be useful also in studies of surface defects (e.g., steps, kinks). The second goal is reported here and involves the exploration of specific effects due to bond-energy variations on segregation in Pt-Pd cluster sites by the combination of the highly efficient statistical-mechanical FCEM and energetics based on the CBEV. The CBEV/FCEM computations without additional adjustable parameters agree very well with previously reported experimental data concerning Pt-Rh(111) oscillatory segregation and this seems to indicate its validity in the Pt-Pd case as well. Two distinct phenomena, dominant Pd subsurface segregation and segregation reversal to Pt at certain surface sites of the Pt-Pd nanoclusters, are due to surface-subsurface and intrasurface preferential bond-energy strengthening, respectively. While the former effect applies for both alloy bulk and alloy cluster subsurfaces, the typical structures of nanoclusters, with several low-coordinated surface sites adjacent to higher-coordinated sites, seems to be a necessary condition for the occurrence of bond-variation-induced segregation reversal (i.e., the reduced bond-breaking driving force at the higher-coordinated site can then be dominated by the two-site bond-energy variation effect).

The present version of the CBEV method is restricted by the use of a limited DFT database of surface energies. By including higher-order polynomials and more DFT-computed elemental- and alloy surface-energy data the method can be further improved. In particular, it is desirable to also take into account the following: (i) possible surface-induced variations in pair interactions beyond NN, (ii) surface-induced variations in the effective heteroatomic interactions, thus extending the applicability of the approach to alloys with relatively strong mixing or demixing tendencies, and (iii) possible multisite interactions. Finally, it should be noted that the importance of the reported results extends beyond the particular alloy system studied to the prospects of such distinct bond-energy-variation effects on segregation in general.

ACKNOWLEDGMENT

This research was supported by The Israel Science Foundation (Grant No.1204/04).

*Corresponding author; mpolak@bgu.ac.il

[1] F. Baletto and R. Ferrando, Rev. Mod. Phys. **77**, 371 (2005).
[2] R. Ferrando, A. Fortunelli, and R. L. Johnston, Phys. Chem. Chem. Phys. **10**, 640 (2008).
[3] M. Polak and L. Rubinovich, Surf. Sci. Rep. **38**, 127 (2000).
[4] Leonid Rubinovich, Michael I. Haftel, Noam Bernstein, and Micha Polak, Phys. Rev. B **74**, 035405 (2006).
[5] Micha Polak and Leonid Rubinovich, Phys. Rev. B **75**, 045415 (2007).
[6] Michael I. Haftel, Noam Bernstein, Michael J. Mehl, and Dimitris A. Papaconstantopoulos, Phys. Rev. B **70**, 125419 (2004).
[7] M. Polak and L. Rubinovich, Int. J. Nanotechnol. (to be published).
[8] C. Barreteau, M. C. Desjonqueres, and D. Spanjaard, Eur. Phys. J. D **11**, 395 (2000).
[9] I. Galanakis, N. Papanikolaou, and P. H. Dederichs, Surf. Sci. **511**, 1 (2002).
[10] C. Mottet, G. Treglia, and B. Legrand, Phys. Rev. B **66**, 045413 (2002).
[11] A. Rapallo, G. Rossi, R. Ferrando, A. Fortunelli, B. C. Curley, L. D. Lloyd, G. M. Tarbuck, and R. L. J. Ohnston, J. Chem. Phys. **122**, 194308 (2005)
[12] M. S. S. Brooks and B. Johansson, J. Phys. F: Met. Phys. **13**, L197 (1983).
[13] Y. J. Wang and J. W. Davenport, Phys. Rev. A **41**, 4690 (1990).
[14] R. Vardi, L. Rubinovich, and M. Polak, Surf. Sci. **602**, 1040 (2008).
[15] J. A. Moriarty, Phys. Rev. B **38**, 3199 (1988).
[16] M. Methfessel, D. Hennig, and M. Scheffler, Phys. Rev. B **46**, 4816 (1992).
[17] T. Futschek, M. Marsman, and J. Hafner, J. Phys.: Condens. Matter **17**, 5927 (2005).
[18] L. Xiao and L. C. Wang, J. Phys. Chem. A **108**, 8605 (2004).
[19] L. O. Paz-Borbon, T. V. Mortimer-Jones, R. L. Johnston, A. Posada-Amarillas, G. Barcaro, and A. Fortunelli, Phys. Chem. Chem. Phys. **9**, 5202 (2007).
[20] Micha Polak and Leonid Rubinovich, Phys. Rev. B **71**, 125426 (2005).
[21] D. Brown, P. D. Quinn, D. P. Woodruff, T. C. Q. Noakes, and P. Bailey, Surf. Sci. **497**, 1 (2002).
[22] S. Muller, M. Stohr, and O. Wieckhorst, Appl. Phys. A: Mater. Sci. Process. **82**, 415 (2006).
[23] Koretaka Yuge, Atsuto Seko, Akihide Kuwabara, Fumiyasu Oba, and Isao Tanaka, Phys. Rev. B **74**, 174202 (2006).
[24] L. Zhu and A. E. DePristo, J. Catal. **167**, 400 (1997).
[25] L. O. Paz-Borbon, R. L. Johnston, G. Barcaro, and A. Fortunelli, J. Chem. Phys. **128**, 134517 (2008).
[26] L. D. Lloyd, R. L. Johnston, S. Salhi, and N. T. Wilson, J. Mater. Chem. **14**, 1691 (2004).
[27] G. E. Ramirez Caballero and P. B. Balbuena, Mol. Simul. **32**, 297 (2005).
[28] J. L. Rousset, J. C. Bertolini, and P. Miegge, Phys. Rev. B **53**, 4947 (1996).
[29] P. L. Hansen, A. M. Molenbroek, and A. V. Ruban, J. Phys. Chem. B **101**, 1861 (1997).
[30] D. J. Cheng, S. P. Huang, and W. C. Wang, Chem. Phys. **330**, 423 (2006).
[31] K. W. Jacobsen, P. Stoltze, and J. K. Norskov, Surf. Sci. **366**, 394 (1996).
[32] O. M. Lovvik, Surf. Sci. **583**, 100 (2005).
[33] D. Radosavkic, N. Barrett, R. Belkhou, N. Marsot, and C. Guillot, Surf. Sci. **516**, 56 (2002).
[34] J. L. Rousset, A. J. Renouprez, and A. M. Cadrot, Phys. Rev. B **58**, 2150 (1998).
[35] C. Kittel, *Introduction to Solid State Physics* (Wiley, New York, 1971).